Acta Mech Sin (2007) 23:173–181
DOI 10.1007/s10409-007-0056-7

RESEARCH PAPER

Mode III fracture analysis by Trefftz boundary element method

Yuhong Cui · Juan Wang · Manicka Dhanasekar · Qinghua Qin

Received: 1 March 2006 / Revised: 14 September 2006 / Accepted: 8 November 2006 / Published online: 21 March 2007

Abstract This paper presents a hybrid Trefftz (HT) boundary element method (BEM) by using two indirect techniques for mode III fracture problems. Two Trefftz complete functions of Laplace equation for normal elements and a special purpose Trefftz function for crack elements are proposed in deriving the Galerkin and the collocation techniques of HT BEM. Then two auxiliary functions are introduced to improve the accuracy of the displacement field near the crack tips, and stress intensity factor (SIF) is evaluated by local crack elements as well. Furthermore, numerical examples are given, including comparisons of the present results with the analytical solution and the other numerical methods, to demonstrate the efficiency for different boundary conditions and to illustrate the convergence influenced by several parameters. It shows that HT BEM by using the Galerkin and the collocation techniques is effective for mode III fracture problems.

Keywords Hybrid Trefftz method · Galerkin technique · Point-collocation technique · Mode III fracture

The project supported by the National Natural Science Foundation of China(10472082). The English text was polished by Keren Wang.

Y. Cui (✉) · J. Wang · Q. Qin
Department of Mechanics, Tianjin University,
Tianjin 300072, China
e-mail: yhcui@tju.edu.cn

J. Wang
e-mail: juan123.wang@yahoo.com.cn

M. Dhanasekar
Centre for Railway Engineering,
Central Queensland University,
North Rockhampton QLD 4702, Australia
e-mail: m.dhanasekar@cqu.edu.au

Q. Qin
Department of Engineering, Australian National University,
Canberra, ACT 0200, Australia
e-mail: qinghua.qin@anu.edu.au

1 Introduction

Since Trefftz [1] in 1926 proposed his approach to deal with boundary conditions by using regular Trefftz functions satisfying the governing equations, many papers have been published [2–8], concerning its fundamentals and applications to some elastic and non-elastic fields. Especially, the concept of HT functions has been found to be useful in dealing with various geometries or load-dependent singularities and local effects [9–12].

With respect to fracture problems, Portela et al. [13] in 1992 first applied this strategy to the potential theory of fracture mechanics using HT method, then planar crack problems were studied by Freitas and Ji [14] in 1996 using the equilibrium element model and by Sabino et al. [15] in 1999 using HT BEM. Their applications show that the Trefftz method is simple and economical, sometimes even better than Somigliana BEM [16]. Furthermore, the input data generation is much easier in HT BEM than the procedures of the finite element method (FEM) [17,18] and the finite difference method. HT BEM is shown to be useful and powerful in comparison with other boundary methods, [13], [19–21]. However, while mode III fracture problems were studied by using HT FEM by the authors recently, HT BEM has not been mentioned.

This paper focuses on two indirect HT BEMs, the Galerkin technique and the collocation technique, for mode III fracture problems. Above all, the original formulations and Trefftz functions satisfying anti-plane crack conditions for normal elements and crack elements are deduced. Then the stiffness matrix and the equivalent nodal flow vector are formed by using the Galerkin method and the collocation method from the approximate solutions in fitting the boundary conditions. In order to improve the accuracy, two auxiliary functions for regions near crack tips are introduced, and a general expression for stress intensity factors (SIF) is obtained based on the special Trefftz function as well. Furthermore, numerical examples are presented to illustrate the application of the proposed approach for finite and infinite boundaries, and to highlight the effect of some important parameters on the numerical accuracy. The results from HT BEM are compared with the analytical solution, and those obtained from other types of BEM and FEM.

2 Basic formulations for mode III fracture problems

2.1 Trefftz complete function for Laplace equation

In the case of anti-plane shear deformation of isotropic solids defined in Cartesian (x_1, x_2 and x_3) coordinates, the displacements in the x_1x_2 plane are zero, i.e., $u_1 = 0$ and $u_2 = 0$, and in the x_3 direction $u_3 = u \neq 0$, where u is the function of x_1 and x_2 only. Hence, the differential governing equation can be written as

$$G\left(\frac{\partial^2 u}{\partial x_1^2} + \frac{\partial^2 u}{\partial x_2^2}\right) = 0, \quad \text{in } \Omega, \tag{1}$$

and the boundary conditions are

$$u = \bar{u} \quad \text{on } \Gamma_u, \quad \text{and} \quad G\frac{\partial u}{\partial n} = \bar{q}, \quad \text{on } \Gamma_q, \tag{2}$$

where G is the shear modulus, u out-of-plane displacement, $\partial u/\partial n$ the unit normal derivative of u, $\Gamma = \Gamma_u + \Gamma_q$ the boundary of the solution domain Ω and an overhead bar denotes the prescribed value. The non-zero stress components are given in terms of the displacement u as

$$\sigma_{31} = G\frac{\partial u}{\partial x_1}, \quad \sigma_{32} = G\frac{\partial u}{\partial x_2}. \tag{3}$$

It is well-known that the solution of Eq. 1 may be found by separating variables, then two Trefftz (T) functions can be obtained as [22]

$$u(r,\theta) = \sum_{m=0}^{\infty} r^m (a_m \cos m\theta + b_m \sin m\theta),$$

$$\text{(for a bounded region)}, \tag{4a}$$

$$u(r,\theta) = a_0^* + a_0 \ln r + \sum_{m=1}^{\infty} r^{-m} (a_m \cos m\theta + b_m \sin m\theta),$$

$$\text{(for an unbounded region)}, \tag{4b}$$

where r and θ are a pair of polar coordinates. Thus, the associated T-complete functions of Eq. (4) can be expressed, respectively, as

$$T = \{1, r^m \cos m\theta, r^m \sin m\theta\} = \{T_i\}, \tag{5a}$$

$$T = \{1, \ln r, r^{-m} \cos m\theta, r^{-m} \sin m\theta\} = \{T_i\}. \tag{5b}$$

2.2 Special Trefftz function for crack elements

A special purpose function can be constructed to satisfy both Laplace equation and the free-traction boundary conditions on crack faces here. The derivation of such functions is based on the general solution of the two dimensional Laplace equation:

$$u(r,\theta) = \alpha_0 + \sum_{n=1}^{\infty} \left(\alpha_n r^{\lambda_n} + \beta_n r^{-\lambda_n}\right) \cos(\lambda_n \theta)$$
$$+ \sum_{n=1}^{\infty} \left(\kappa_n r^{\beta_n} + \zeta_n r^{-\gamma_n}\right) \sin(\gamma_n \theta), \tag{6}$$

where λ_n and γ_n are two sets of constants which are assumed to be greater than zero. An appropriate trial function for a singular corner element is obtained by considering an infinite wedge (Fig. 1) with particular boundary conditions prescribed along the sides $\theta = \theta_0$ forming an angular corner. The boundary condition for the wedge is

$$\frac{\partial u}{\partial \theta} = 0, \quad (\text{for } \theta = \pm\theta_0). \tag{7}$$

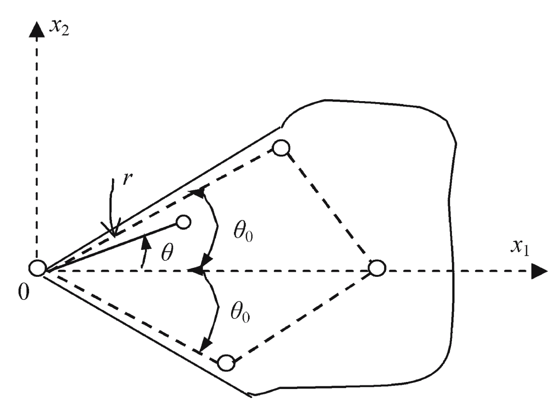

Fig. 1 A singular corner element for an infinite wedge

Differentiating (6) and substituting it into Eq. 7, we obtain

$$\frac{\partial u}{\partial \theta}\Big|_{\theta=\pm\theta_0} = -\sum_{n=1}^{\infty} \lambda_n\left(\alpha_n r^{\lambda_n} + \beta_n r^{-\lambda_n}\right)\sin(\pm\lambda_n\theta_0) + \sum_{n=1}^{\infty} \gamma_n\left(\kappa_n r^{\gamma_n} + \zeta_n r^{-\gamma_n}\right)\cos(\pm\gamma_n\theta_0) = 0. \tag{8}$$

Since it assumes a limited value at $r = 0$, we have $\beta_n = \zeta_n = 0$ and then

$$\sin(\pm\lambda_n\theta_0) = 0, \quad \cos(\pm\gamma_n\theta_0) = 0, \tag{9}$$

which means that

$$\begin{aligned} &\lambda_n\theta_0 = n\pi, \quad (n = 1, 2, 3, \ldots), \\ &2\gamma_n\theta_0 = n\pi, \quad (n = 1, 3, 5, \ldots), \end{aligned} \tag{10}$$

Thus, the final form of the solution when $\theta_0 = \pi$ is

$$u(r,\theta) = \alpha_0 + \sum_{n=1}^{\infty} \alpha_n r^n \cos(n\theta) + \sum_{n=1,3,5}^{\infty} \kappa_n r^{n/2} \sin\left(\frac{n}{2}\theta\right). \tag{11}$$

It is obvious that the displacement function (11) includes the term proportional to $r^{1/2}$, whose derivative is singular at the crack tip.

2.3 Assumed element displacement field of HT BEM

The element matrix can be derived based on assumed elemental displacement fields, and the solution domain Ω is divided into the interior domain and the problem (or boundary) domain that scales into a circle of unit radius. For Trefftz BEM, the eigen functions of Eq. 1 in an interior element displacement domain "e" can be expressed by

$$\boldsymbol{u}_{\mathrm{e}} = \boldsymbol{u}_{\mathrm{e}}^{*}\boldsymbol{c}, \tag{12}$$

where $\boldsymbol{c}$ is a vector of undetermined coefficients, $\boldsymbol{u}_{\mathrm{e}}^{*}$ is homogeneous solutions to the governing equation of boundary element field. Noting that T-function in Eq. 5a satisfies Eq. 1, $\boldsymbol{u}_{\mathrm{e}}^{*}$ can be defined as

$$u_{ei}^{*} = T_i, \quad (i = 1, 2, \ldots, n). \tag{13}$$

Hereafter, to further simplify the writing, we shall omit the subscript "e" in related expressions when the distinction is unnecessary. That is

$$\boldsymbol{u} = \boldsymbol{u}^{*}\boldsymbol{c}. \tag{14}$$

With solution (11), the internal function defined in Eq. 14 takes the form:

$$\begin{aligned} &u_{2n-1}^{*} = r^n \cos(n\theta), \\ &u_{2n}^{*} = r^{\frac{(2n-1)}{2}} \sin\left(\frac{(2n-1)}{2}\theta\right), \\ &\quad (n = 1, 2, 3, \ldots). \end{aligned} \tag{15}$$

3 Weighted residual formulations of HT BEM

According to the general formulation of weighted techniques, Eqs. 1 and 2 lead to the integral equation:

$$\int_{\Omega} (\nabla^2 \boldsymbol{u})\boldsymbol{W}_{\Omega}\mathrm{d}\Omega + \int_{\Gamma_u} (\boldsymbol{u} - \bar{\boldsymbol{u}})\boldsymbol{W}_u \mathrm{d}\Gamma + \int_{\Gamma_q} (\boldsymbol{q} - \bar{\boldsymbol{q}})\boldsymbol{W}_q \mathrm{d}\Gamma = 0, \tag{16}$$

where $\boldsymbol{W}_{\Omega}, \boldsymbol{W}_u, \boldsymbol{W}_q$ are certain weighting functions defined in Ω, Γ_u and Γ_q, respectively. For Trefftz BEM, u is an approximated function satisfying Eq. 1, but not necessarily Eqs. 2, hence, Eq. 16 is reduced to

$$\int_{\Gamma_u} (\boldsymbol{u} - \bar{\boldsymbol{u}})\boldsymbol{W}_u \mathrm{d}\Gamma + \int_{\Gamma_q} (\boldsymbol{q} - \bar{\boldsymbol{q}})\boldsymbol{W}_q \mathrm{d}\Gamma = 0. \tag{17}$$

The function $\boldsymbol{u}$ can be expressed by Trefftz functions as the retained several terms, thus at a point P, $\boldsymbol{u}$ and $\boldsymbol{q}$ can be expressed, respectively, as

$$\begin{aligned} &\boldsymbol{u}(P) \approx c_i u_i^{*} = \boldsymbol{u}^{*\mathrm{T}}\boldsymbol{c}, \\ &\boldsymbol{q}(P) = \frac{\partial}{\partial n}\boldsymbol{u}(P)^{*} \approx c_i \frac{\partial}{\partial n} u_i^{*} = \boldsymbol{q}^{*\mathrm{T}}\boldsymbol{c}, \end{aligned} \tag{18}$$

in which $\boldsymbol{c}$ is a vector of unknown parameters that correspond to the terms considered in the expansions of Trefftz functions. Particularly, the weighting functions $\boldsymbol{W}_u$ and $\boldsymbol{W}_q$ can be chosen in special ways that Eq. 17 can lead to the Galerkin approach and the collocation approach, respectively.

3.1 The point-collocation formulations of HT BEM

The point-collocation formulations can be obtained when the weighting functions are chosen to be the Dirac delta function as:

$$W_u = W_q = \delta(P - P_i), \tag{19}$$

where P_i is the collocation point. Then Eq. 18 leads to equations:

$$\boldsymbol{u}(P_i) = \boldsymbol{u}^{*\mathrm{T}}\boldsymbol{c} = \bar{\boldsymbol{u}}(P_i), \quad \text{for } P_i \text{ on } \Gamma_u, \tag{20a}$$

$$\boldsymbol{q}(P_i) = \boldsymbol{q}^{*\mathrm{T}}\boldsymbol{c} = \bar{\boldsymbol{q}}(P_i), \quad \text{for } P_i \text{ on } \Gamma_q., \tag{20b}$$

Equations (20) can be further written as:

$$K_{ij}c_j = f_i, \tag{21}$$

where the unknown parameter c_j represents the constant coefficient of the jth term of the Trefftz functions, the coefficient K_{ij} and the term f_i are given, respectively, as

$$K_{ij} = u_j^*(P_i) \quad \text{or} \quad K_{ij} = q_i^*(P_i), \tag{22a}$$

$$f_i = \bar{u}(P_i) \quad \text{or} \quad f_i = \bar{q}(P_i). \tag{22b}$$

For a set of collocation points, Eq. 21 can be written in matrix form as:

$$\boldsymbol{Kc} = \boldsymbol{f}. \tag{23}$$

3.2 The Galerkin formulations of HT BEM

Similar to the point-collocation method above, the Galerkin formulations can be obtained when the weighting functions are defined as:

$$W_u = \delta q = \boldsymbol{q}^{*\mathrm{T}}\delta\boldsymbol{c}, \quad W_q = -\delta u = -\boldsymbol{u}^{*\mathrm{T}}\delta\boldsymbol{c}. \tag{24}$$

In this case, Eq. 17 leads to:

$$\begin{aligned} &\delta\boldsymbol{c}^{\mathrm{T}}\Big\{\int_{\Gamma_u}\boldsymbol{q}^*\boldsymbol{u}^{*\mathrm{T}}\mathrm{d}\Gamma - \int_{\Gamma_q}\boldsymbol{u}^*\boldsymbol{q}^{*\mathrm{T}}\mathrm{d}\Gamma\Big\}\boldsymbol{c} \\ &\quad = \int_{\Gamma_u}\boldsymbol{q}^*\bar{\boldsymbol{u}}\mathrm{d}\Gamma - \int_{\Gamma_q}\boldsymbol{u}^*\bar{\boldsymbol{q}}\mathrm{d}\Gamma = 0 \\ &\quad \Rightarrow \Big\{\int_{\Gamma_u}\boldsymbol{q}^*\boldsymbol{u}^{*\mathrm{T}}\mathrm{d}\Gamma - \int_{\Gamma_q}\boldsymbol{u}^*\boldsymbol{q}^{*\mathrm{T}}\mathrm{d}\Gamma\Big\}\boldsymbol{c} \\ &\quad = \int_{\Gamma_u}\boldsymbol{q}^*\bar{\boldsymbol{u}}\mathrm{d}\Gamma - \int_{\Gamma_q}\boldsymbol{u}^*\bar{q}\mathrm{d}\Gamma. \end{aligned} \tag{25}$$

The final equations can also be written in matrix form as Eq. 23, in which the coefficients and the independent terms are given by:

$$K_{ij} = \int_{\Gamma_u} q_i^*u_j^*\mathrm{d}\Gamma - \int_{\Gamma_q} u_i^*q_j^*\mathrm{d}\Gamma, \tag{26a}$$

$$f_i = \int_{\Gamma_u} q_i^*\bar{u}_j\mathrm{d}\Gamma - \int_{\Gamma_q} u_i^*\bar{q}_j\mathrm{d}\Gamma. \tag{26b}$$

Noting that the resulting equation for both Galerkin and the collocation methods is in the same form of Eq. 23, where K_{ij} and f_i are, respectively, coefficients of the stiffness matrix and a known force vector, obtained by integrating along the boundaries of elements. Since the matrix of the coefficients is symmetric, an important character in Galerkin method is that,

$$q_i^* = \frac{\partial}{\partial n}u_i^*. \tag{27}$$

4 Two auxiliary functions for the singular property near crack tips

The special function (Eq. 11) is constructed by use of both Eq. 1 and the free-traction boundary condition (7) on crack faces. However, the function cannot accurately represent the singular property near crack tips due to

$$\frac{\partial u}{\partial \theta} \neq 0 \quad (\text{for } \theta = \pm\theta_0) \quad \text{when } x_1 = 0 \text{ and } x_2 = 0. \tag{28}$$

Furthermore, their boundary functions should sharply vary from $x_1 > 0$ and $x_2 = 0$ to $x_1 < 0$ and $x_2 = 0$ near crack tips. That is to say, those two conditions are not both satisfied completely in fact. Therefore, the term $\partial u/\partial\theta$ makes no contribution to the stiffness matrix and equivalent nodal flow vector in Eq. 21 if the elements contain crack tips due to Eq. 7. Hence, Eq. 7 makes no contribution to the computation of SIF. We will provide a solution, to this problem.

As is known, SIF is obtained by considering the special stress distribution around the crack tip $x_1 = 0$ and $x_2 = 0$. An exact function to satisfy the feature near the crack-tip becomes an important factor for computing accuracy. Therefore, according to the particular boundary condition of Eq. 28, the displacements and stresses prescribed along both sides of $x_1 = 0$ and $x_2 = 0$ should be completely equivalent within a very small region around crack tip, called the micro size region, and the displacements and stresses at one side along $x_1 < 0$ and $x_2 = 0$ can be deduced from the results of the other side $x_1 > 0$ and $x_2 = 0$ using some approximate approaches reported in the literature [8,13,15].

From this point of view, the paper presents a calculating approach, namely, an auxiliary function approach, in which the displacements satisfy the singular property near crack tips. In this approach, the displacements and stresses along the left micro size region of $x_1 = 0$ and $x_2 = 0$ are expressed in terms of some analytical functions, which can simulate the characters along the right micro size region. Meanwhile, the auxiliary function also approximately agrees with Eq. 1 and the boundary condition Eq. 28 around the micro region. In fact, these auxiliary functions can be found easily, such as the two following expressions

$$q_{\text{tip}} = \frac{\zeta}{L^\alpha}(r^\alpha - L^\alpha)\cos\theta, \quad \alpha < 1.0, \tag{29}$$

$$q_{\text{tip}} = \frac{\zeta}{L^\alpha}(L - r)^\alpha\cos\theta, \quad \alpha \geq 1.0, \tag{30}$$

which are used in the calculation, and the equation of force equilibrium

$$\int_0^L \zeta\,\mathrm{d}x = \int_{\Gamma_q} q_{\text{tip}}\mathrm{d}\Gamma$$

is used to determine the unknown value ζ, while L is the crack length and α the power parameter of the functions.

Two advantages using the auxiliary functions can be seen clearly, one is that the accuracy can be improved near crack tips when the computation involves a region far from crack tips; another is that slight different results can be achieved using different auxiliary functions, in spite of different convergence situations for different functions. That is to say, this feature can be applied to check the correctness of the outcomes as well.

5 Singular intensity factor of Trefftz BEM

On the basis of the special function for crack elements, SIF K_{III} can be evaluated from c_i straightforwardly. Since the general expression of SIF can be given as

$$K_{\text{III}} = \lim_{r\to 0}\left[\frac{(2\pi)^{1/2}}{r^{1-\lambda}}\sigma_{32}(r, 0)\right], \tag{31}$$

where $\lambda = 1 - \frac{\pi}{2\theta_0}$ when $\theta_0 \neq \pi$, the singularity is the type of $r^{\lambda-1}$. When the cracks tip is defined at the origin of the polar coordinate system (see Fig. 1), substituting Eq. 3 and Eq. 14 into Eq. 31, one obtains

$$K_{\text{III}} = \lim_{r\to 0}\frac{(2\pi)^{1/2}}{r^{1-\lambda}}G\frac{\partial u^*}{\partial x_2}c = \lim_{r\to 0}\frac{(2\pi)^{1/2}}{r^{1-\lambda}}G\Big(\frac{\partial u_1^*}{\partial\theta}c_1 + \frac{\partial u_2^*}{\partial\theta}c_2 + \frac{\partial u_3^*}{\partial\theta}c_3 + \frac{\partial u_4^*}{\partial\theta}c_4 + \frac{\partial u_5^*}{\partial\theta}c_5 + \ldots\Big),$$

that is,

$$K_{\text{III}} = \sqrt{2\pi}\,\mathrm{G}c_3\frac{\pi}{2\theta_0}. \tag{32}$$

When $\theta = 180°$, the T-complete system solution is footnotesize

$$\frac{\partial u^*}{\partial\theta} \in \Big\{0, -r\sin\theta, \frac{1}{2}r^{1/2}\cos\frac{\theta}{2}, -2r^2\sin 2\theta, \frac{3}{2}r^{3/2}\cos\frac{3}{2}\theta, \ldots\Big\},$$

hence SIF can be written as

$$K_{\text{III}} = \sqrt{\frac{\pi}{2}}Gc_3. \tag{33}$$

Generally speaking, SIF can be evaluated by local field distributions of c_i at crack tips.

6 Numerical assessments

6.1 A rectangular plate with finite boundaries for mode III edge crack

Figure 2 shows a rectangular plate with finite edges for mode III edge crack to numerically illustrate the HT BEM. Due to symmetric conditions, only half of the plate is meshed as shown in Fig. 2. The boundary

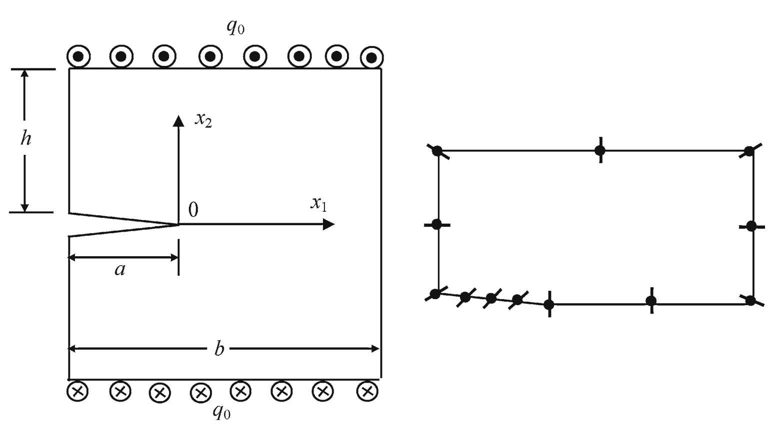

Fig. 2 A rectangular plate with finite edges for mode III edge crack and its meshing

conditions of the problem are

$$
\begin{aligned}
&x_2 = 0, \quad x_1 < 0, \quad \sigma_{32} = 0; \\
&x_2 = 0, \quad x_1 \geq 0, \quad u = 0; \\
&-h \leq x_2 \leq h, \quad x_1 = -a \\
&\text{and } x_1 = (b-a), \quad \sigma_{31} = 0; \\
&x_2 = \pm h, \quad -a \leq x_1 \leq (b-a), \quad \sigma_{32} = \pm q_0.
\end{aligned} \tag{34}
$$

Boundary quadratic elements are used along the uncracked (regular) edges while higher order elements are used in the cracked edge, and a higher mesh density is assumed in the region containing the crack. It should be indicated that a local coordinate system is adopted to avoid developing ill-conditioned matrices and a singular value decomposition solver is incorporated in the solution algorithm. The ratio a/b is taken to be 0.1, 0.5, 0.9 and $\theta_0 = 180°$ in the analysis. Moreover, the auxiliary functions used are defined by Eq. 29 and Eq. 30 in both Galerkin approach and collocation approach.

Table 1 shows the results of SIF versus the number of special T-functions for the mode III crack problem when $a/b = 0.5$. It is found that the ratio K/K_c (K is the SIF by the present computation and K_c is as defined in Refs. [28,23] gradually decreases when the number of special T-functions increases, then converges to 0.971 when the number of special T-functions ≥ 6 for Eq. 29 and it converges to 0.910 when the number of special T-functions = 4 for Eq. 30 as in the Galerkin approach, whereas it converges to 0.988 for Eq. 29 and 0.910 for Eq. 30 when the number of special T-functions ≥ 6 as in the collocation approach. Furthermore, the choice of two auxiliary functions appears to have an effect on the value K determined, and Eq. 29 consistently yields higher converged value with respect to Eq. 30 in HT BEM. However, there is very little difference between the collocation approach and the Galerkin approach for the rate of convergence irrespective of the type of the auxiliary functions used.

The results of SIF K/K_c versus the number of crack elements are listed in Table 2. It indicates that the ratio K/K_c converges to a stable value with the increase of the number of crack elements, the convergence in this case is in a similar manner as with respect to the number of T-function terms. Once again both the collocation approach and the Galerkin approach perform similarly, and the converged values in Table 2 are identical to the values in Table 1.

The effect of the collocation point number to the K/K_c ratio is shown in Table 3. It can be seen that the ratio converges to 0.988 when the collocation point number = 10 for Eq. 29, whilst the ratio remains at the converged level (0.945) even when the collocation point number = 4 for Eq. 30. From the table, it can also be seen that the auxiliary functions of Eq. 29 can provide a more

Table 1 SIF K/K_c versus the number of special T-functions ($a/b = 0.5$)

Two indirect approaches		Number of special T-functions				
of HT BEM		2	4	6	8	10
Galerkin approach	Eq. 29	1.672	0.972	0.971	0.971	0.971
	Eq. 30	1.567	0.910	0.910	0.910	0.910
Point-collocation approach	Eq. 29	1.701	0.989	0.988	0.988	0.988
	Eq. 30	1.627	0.946	0.945	0.945	0.945

Table 2 SIF K/K_c versus the number of crack elements ($a/b = 0.5$)

Two indirect approaches		Number of special T-function				
of HT BEM		2	4	6	8	10
Galerkin approach	Eq. 29	1.047	0.990	0.971	0.971	0.971
	Eq. 30	0.910	0.910	0.910	0.910	0.910
Point-collocation approach	Eq. 29	1.116	1.031	0.988	0.988	0.988
	Eq. 30	0.948	0.946	0.945	0.945	0.945

Table 3 SIF K/K_c versus the number of collocation points and Gauss points ($a/b = 0.5$)

Indirect approach of HT BEM		Galerkin or Point-collocation approach				
		2	4	6	8	10
Number of collocation points	0.954	0.954	0.976	0.982	0.986	0.988
	0.945	0.946	0.945	0.945	0.945	0.945
Number of Gauss points	0.984	0.984	0.971	0.970	0.970	0.970
	0.892	0.892	0.910	0.910	0.910	0.910

stable solution than those of Eq. 30. Furthermore, the number of Gauss points for the Galerkin approach has an influence on the results, as shown in Table 3, and the K/K_c ratio converges to a stable value when the number of Gauss points grows and converges to 0.971 for Eq. 29 and 0.910 for Eq. 30 when the number of special T-functions ≥ 4.

The results for the same mode III problem were obtained from HT FEM [17], which are compared with HT BEM, as shown in Figs. 3 and 4. Generally, the converged values of the ratio K/K_c obtained from HT FEM are slightly larger (not very significantly) than those obtained from HT BEM. Although both approaches can provide similar convergent results, the present HT BEM offers a significant computational advantage in terms of reduced DOF. On the other hand, as it can be seen from the figures, the difference between HT FEM and HT BEM on the convergence performance versus either the number of special T-functions or the number of crack elements is not significant.

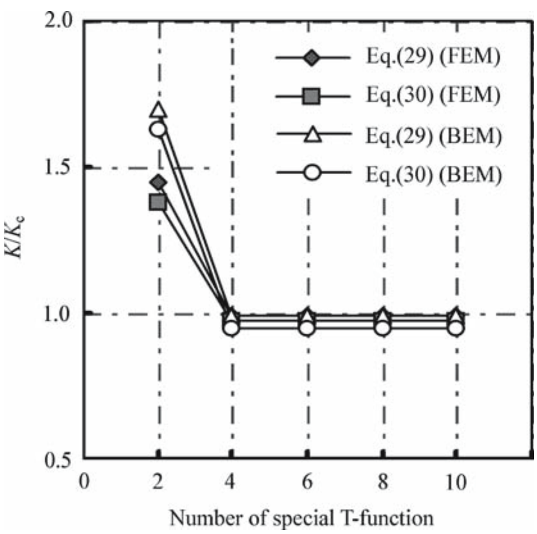

Fig. 3 SIF versus the number of special T-functions (FEM and BEM)

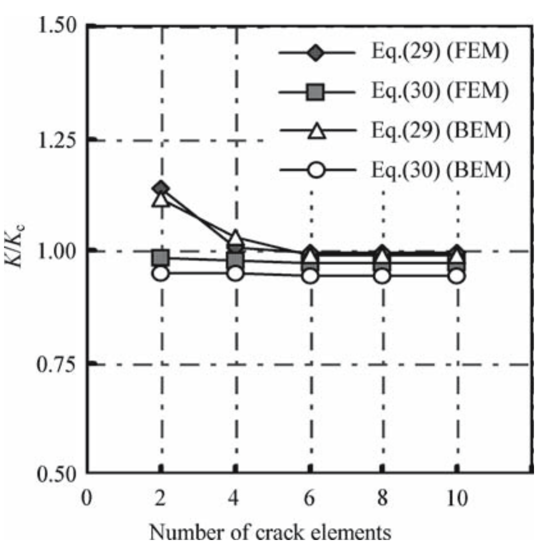

Fig. 4 SIF versus the number of crack elements (FEM and BEM)

Furthermore, some particular solutions for a crack in a rectangular plane were obtained by Isida [24] using a perturbation technique, by Rooke [23] using a versatile method and by Sih [25] using the Cagniard's technique. In particular, Silling [26] developed an APE program to calculate stress concentration factors, then Honrgan and Silling [27] using a finite-difference program assessed the accuracy of direct numerical computations for the finite anti-plane shear problem by comparing the corresponding analytical results. They found that each of the circular meshes used for the elliptical cavity with a traction-free boundary contained roughly 1,000 nodes to obtain results with no more than 2% error for linear cases and 1% for nonlinear cases, as compared with the exact analytical value. However, we use less than 10 elements and 30 nodes for HT BEM and 15 elements and 40 nodes for HT FEM calculating for an edge crack of the rectangular plate for the mode III problem, to achieve the same goal. This further illustrates the efficiency of the proposed HT BEM/HT FEM over the other traditional methods.

6.2 A rectangular plate with infinite boundaries for mode III three edge cracks

The second example is a rectangular plate with infinite boundaries with three edge cracks (Fig. 5). The ratio of $a/2c$ is fixed at 3, and the length of b and h are taken as 6 times of a to eliminate influence on the results by the boundary conditions. Owing to the symmetric conditions, only half of the plate is meshed as shown in Fig. 5. The boundary conditions of the problem are

$$\begin{aligned}
&y = 0, x < 0 \quad \text{and} \quad y = c, x < 0, \sigma_{32} = 0;\\
&y = 0 \quad \text{and} \quad x \geq 0, \quad u = 0;\\
&-h/2 \leq y \leq h/2 \quad \text{and} \quad x = -a;\\
&x = (b - a), \quad \sigma_{31} = 0;\\
&y = \pm h/2 \quad \text{and} \quad -a \leq x \leq (b - a), \quad \sigma_{32} = \pm q_0.
\end{aligned} \tag{35}$$

Equation (29) is also used as the auxiliary equation only, and the normalized stress intensity factors $K/q_0\sqrt{\pi a}$ at points O and O' are calculated. As to the rank condition, the number of T-functions should be ≥ 3 for regular elements and ≥ 6 for special purpose elements in the calculation.

Table 4 shows the results of normalized stress intensity factors $K/q_0\sqrt{\pi a}$ versus the number of special

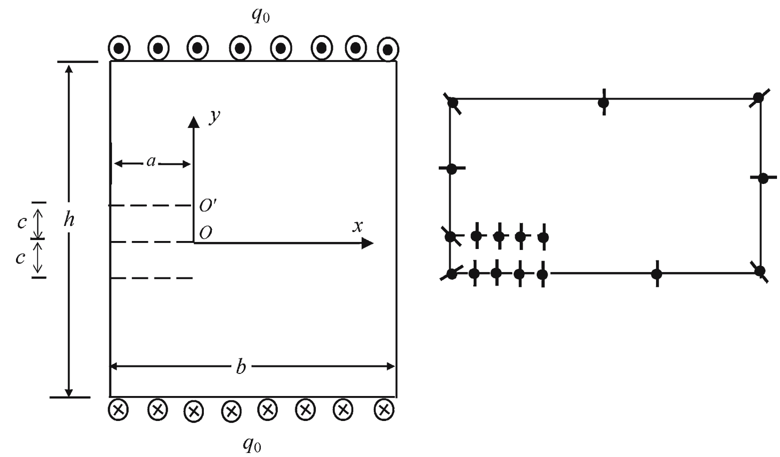

Fig. 5 A rectangular plate with infinite boundaries for mode III three edge cracks and its meshing

Table 4 Normalized SIF $K/q_0\sqrt{\pi a}$ versus the numbers of crack elements and special T-functions for a multi-crack plate ($a/2b = 3$)

Number of crack elements	Number of special T-functions	O point	O' point
4	2	0.463	0.451
6	3	0.337	0.343
10	4	0.329	0.338
12	5	0.329	0.338

T-functions and the number of crack elements for three edge-crack infinite plate. The ratio $K/q_0\sqrt{\pi a}$ gradually decreases when the number of special T-functions and the number of crack elements increase, then converges to 0.329 for point O' and 0.338 for point O, respectively, while the number of special T-functions $\geq$ 4 and the number of crack elements $\geq$ 10. The convergence due to the increase of the number of special Trefftz-functions is also considered good for the multi-crack problem.

The normalized stress intensity factors $K/q_0\sqrt{\pi a}$ at points O and O' for different values of $a/2b$ are presented in Table 5. It can be seen that the ratio $K/q_0\sqrt{\pi a}$ for points O and O' decreases with $a/2b$ increasing. However, they are a little larger than the theoretical value [25] and the results obtained by ABQUAS software are less than those of FEM [18]. As a matter of fact, the errors of the results by HT BEM are no more than 1.9 and 3.7% for point O and point O', respectively. The main reason may be that the boundary conditions of the theoretical analysis based on b and h are both for infinite lengthes, in the meanwhile, by ABQUAS software used almost 26,000 nodes and HT FEM 38 nodes whereas HT BEM only 32 nodes.

It should be mentioned that, with the basic theorem of the Fourier transform and Fourier series, the general analytical solutions of SIF subjected to anti-plane shear load were obtained by many researchers, such as Refs. [28,29], but they are almost predetermined by the conditions of infinite edges or special boundaries. The numerical calculations in this paper are for certain finite edges or finite boundaries.

7 Conclusions

HT BEM based on the Galerkin and collocation techniques for mode III fracture problems is presented in the paper. The formulations of HT indirect methods are derived using T-complete functions for normal elements and special T-functions for crack elements, and two auxiliary functions are also adopted to improve the accuracy in crack-tip elements. Meanwhile, its SIF can be evaluated directly by c_3 in crack tips. The performance of the special purpose element model is assessed

Table 5 Normalized SIF $K/q_0\sqrt{\pi a}$ varying with $a/2b$ for a multi-crack plate

Approach	Position	$a/2b$				
		1	2	3	4	5
HT BEM	point O	0.570	0.403	0.329	0.286	0.257
	point O'	0.581	0.410	0.338	0.292	0.258
HT FEM [21]	point O	0.576	0.410	0.335	0.290	0.255
	point O'	0.582	0.413	0.340	0.295	0.265
ABQUAS Software	point O	0.568	0.401	0.327	0.284	0.256
	point O'	0.579	0.407	0.336	0.291	0.267
Theory value[31] ($a \gg b$)	point O or O'	0.563	0.399	0.326	0.282	0.252

by two examples using two indirect approaches. It is found that SIF is affected by the number of special T-functions, the number of crack elements, the number of collocation points, the number of Gauss points and their positions in the edge cracks. Moreover, the ratios K/K_c and $K/q_0\sqrt{\pi a}$ converge to a stable value when the numbers of crack elements, special T-functions and collocation points increase, and SIF converges approximately to the same value irrespective of the type of the auxiliary functions chosen.

The numerical results are compared with those obtained by the conventional FEM/BEM, ABQUAS software and HT FEM. The comparisons show that the proposed Trefftz BEM is ideally suited for the analysis of mode III fracture problems with high efficiency whereas the procedure is usually complicated and time-consuming using the conventional FEM and BEM.

To further assess the performance of the proposed element model, the displacement and stress fields in some selected elements and nodes are analyzed, particularly at the nodes between the crack elements and regular elements. When using the auxiliary functions, the accuracy of displacements and stresses in the left and right sides of micro size region around $x_1 = 0$ and $x_2 = 0$ is about 10^{-3}, while the corresponding accuracy for those points far from $x_1 = 0$ and $x_2 = 0$ is about 10^{-2}. When the regular elements are used, the precision of 10^{-8} to 10^{-10} can be obtained in this example, which is much higher than that of the crack elements. It is also evident that the accuracy is much higher than that of the conventional finite element model or other approaches when the numbers of elements and nodes employed are the same.

References

1. Trefftz, T.E.: Ein Gegenstück zum Ritzschen Verfahren. In: Proceedings 2nd International Congress of Applied mechanics, Zurich, pp. 131–137 (1926)
2. Huang, S.C., Shaw, R.P.: The Trefftz method as an internal equation. Adv. Eng. Softw. **24**, 57–63 (1995)
3. Mikhlin, S.G.: Variational Methods in Mathematical Physics. Pergamon Press, Oxford (1964)
4. Kupradze, V.D.: Three Dimensional Problems of the Mathematical Theory of Elasticity and Thermoelasticity. North Holland, Amsterdam (1979)
5. Piltner, R.: Rencent developments in the Trefftz method for finite element and boundary element applications. Adv. Eng. Softw. **24**, 107–115 (1995)
6. Zienkiewicz, O.C.: Trefftz type of approximation and the finite element method—history and development. In: First International Workshop on Trefftz Method—Recent Development and Perspectives. Cracow University of Technology, Poland, pp. 103 (1996)
7. Jirousek, J., Zielinski, A.P.: Survey of Trefftz-type element formulations. In: First International Workshop on Trefftz Method—Recent Development and Perspectives. Cracow University of Technology, Poland, pp. 103 (1996)
8. Qin, Q.H.: The Trefftz Finite and Boundary Element Method. WIT Press, Southampton (2000)
9. Jirousek, J., Venkatesh, A.: Hybrid-Trefftz plane elasticity elements with p-method capabilities. Int. J. Numer. Meth. Eng. **35**, 1443–1472 (1992)
10. Piltner, R.: Special finite elements with holes and internal cracks. Int. J. Numer. Meth. Eng. **21**, 1471–1485 (1985)
11. Venkatesh, A., Jirousek, J.: Accurate representation of local effect due to concentrated and discontinuous loads in hybrid-Trefftz plate bending elements. Comput. Struct. **57**, 863–870 (1995)
12. Jirousek, J., Teodorescu, P.: Large finite elements method for the solution of problems in the theory of elasticity. Comput. Struct. **15**, 575–587 (1982)
13. Portela, A., Aliabadi, M.H., Rooke, D.P.: The dual boundary element method: effective implementation for crack problems. Int. J. Numer. Methods Eng. **33**, 1269–1287 (1992)
14. Freitas, J.A.T., Ji, Z.Y.: Hybrid-Trefftz equilibrium model for crack problems. Int. J. Numer. Meth. Eng. **39**, 569–584 (1996)
15. Sabino, J., Portela, A., Castro, P.M.S.T.: Trefftz boundary element method applied to fracture mechanics. Eng. Frac. Mech. **64**, 67–86 (1999)
16. Gray, L.J.: Boundary Element Method for Regions with Thin Interal Cavities. IBM Bergen, Norway (1987)
17. Cui, Y.H., Qin, Q.H.: Discussion on anti-plane crack problems by hybrid Trefftz finite element approach. Acta Mech. Solida Sinica, **27**, 167–174 (2006)
18. Cui, Y.H., Qin, Q.H., Wang, J.S.: Application of HT finite element approach on mode I, II and III complex problems. Eng. Mech. **23**, 104–110 (2006)
19. Portela, A., Charafi, A.: Porgramming Trefftz boundary elements. Adv. Eng. Softw. **28**, 509–523 (1997)
20. Leitão, V.M.A.: Applications of multi-region Trefftz-collocation to fracture mechanics. Eng. Anal. Bound. Elem. **22**, 251–256 (1998)
21. Domingues, J.S., Portela, A., Castro, P.M.S.T.: Trefftz boundary element method applied to fracture mechanics. Eng. Fract. Mech. **64**, 67–86 (1999)
22. Zielinski, A.P., Zienkiewicz, O.C.: Generalized finite element analysis with T-complete boundary solution functions. Int. J. Numer. Meth. Eng. **21**, 509–528 (1985)
23. Rooke, D.P., Cartwright, D.S.: Compendium of Stress Intensity Factors. HerMajestys Stationery Office, London (1976)
24. Isida, M.: Analysis of stress intensity factors for plates containing a random array of cracks. Bull JSME **13**, 635–642 (1970)
25. Sih, C.G.: Handbook of Stress Intensity Factors. HerMajestys Stationery Office, London (1973)
26. Silling, S.A.: Singularities and phase transitions in elastic solids: numerical studies and stability analysis. (Ph. D. thesis), California Institute of Technology (1986)
27. Horgan, C.O., Silling, S.A.: Stress concentration factors in finite anti-plane shear numerical calculations and analytical estimates. J. Elast. **18**, 83–91 (1987)
28. Zhang, X.S.: Thegeneral solution of an edge crack off the center line of a rectangular sheet for Mode III. Eng. Fract. Mech. **31**, 847–855 (1988)
29. Sun, Y.Z., Yang, S.S., Wang, Y.B.: A new formulation of boundary element method for cracked anisotropic bodies under anti-plane shear. Comput. Methods Appl. Mech. Eng. **192**, 2633–2648 (2003)